Int. J. Electrochem. Sci., 8 **(2013)** 4036 - 4046

International Journal of
ELECTROCHEMICAL
SCIENCE
www.electrochemsci.org

Formation and Characterization of Cobalt Aluminate Nano-Particles

N. M. Deraz[*]

Chemistry Department , College of Science, King Saud University, P.O. Box 2455, Riyadh 11451, Saudi Arabia
*E-mail: nmderaz@yahoo.com

Received: 14 December 2012 / *Accepted:* 9 February 2013 / *Published:* 1 March 2013

Various structural properties of cobalt aluminates such as crystallite size, lattice constant, unit cell volume, X-ray density, cation distribution of were determined by X-ray diffraction (XRD) and infrared (IR) techniques. Cobalt aluminates were prepared in this study by combustion route. The morphological properties of cobalt aluminates and the surface concentration of elements of these aluminates were studied by Scanning electron micrographs (SEM) and Energy dispersive X-ray (EDX) techniques. The results revealed that the method investigated led to formation of single phase of well crystalline cobalt aluminates ($CoAl_2O_4$) with spinel structure. The as synthesized powders were spongy and fragile. The change in amount of fuel used in the combustion method affects formation and crysatllinity of cobalt aluminates.

Keywords: XRD; SEM, EDX; $CoAl_2O_4$ nano- particles.

1. INTRODUCTION

Solid state reaction of cobalt and aluminum oxides is the most widely used method for the preparation of polycrystalline aluminates [1- 3]. High mobility of the reactants and maximum contact surface between the reactivity particles are desirable to proceed solid state reaction within a reasonable period of time. Raising the temperature or forming a more reactive precursor resulted in an increase in the rate of diffusion and reactivity of the reacting components with subsequent increase in the rate of solid state reaction [4, 5]. Thus we can be seen that this method is usually a complex one that depends on the surface area as well as the defect structure. However, the formation of a product tends to reduce the area of contact between reactants and also to reduce the rate of reaction. In other words, the extent of product formation is influenced by the area of interfacial contact and the ease of diffusion through a product layer. In addition, the diffusion of reactants through a product layer depends on temperature,

defect structure of this layer, grain boundary contacts, presence of impurities and effectiveness of phase boundary contacts [1].

Aluminates are used in different technological applications such as high density magnetic recording, microwave devices, magnetic fluids, heterogeneous catalysis, absorbent materials and pigment industries [6-8]. Conventional preparation of aluminates requires the heat treatment for a mixture of the corresponding oxides [9]. Chemical co-precipitation, sol–gel, polymeric precursor and hydrothermal treatment are various preparation methods for the synthesis of nano-sized aluminates [10-14]. Spinel materials can be prepared by glycine assisted combustion route [15, 16]. It was found to be a good method for preparation the spinel materials in a short time with high-purity, homogeneity and well crystalline products. So, this method was found to be preparing nano-sized cobalt aluminate powders with a broad range of particle sizes.

In the current study, we aim to prepare cobalt aluminates via glycine-assisted combustion method. Another goal for this investigation is the study of the effect of glycine content on the structural and morphological properties of the as prepared cobalt aluminates. The techniques employed were XRD, IR, EDX and SEM.

2. EXPERIMENTAL

2.1. Materials

Four samples of Co/Al mixed oxides were prepared by mixing calculated proportions of cobalt and aluminum nitrates with different amounts of glycine. The mixed precursors were concentrated in a porcelain crucible on a hot plate at 350 ^{o}C for 5 minutes. The crystal water was gradually vaporized during heating and when a crucible temperature was reached, a great deal of foams produced and spark appeared at one corner which spread through the mass, yielding a brown voluminous and fluffy product in the container. In our experiment, the ratios of the glycine: aluminum: cobalt nitrates were (0, 2, 4, and 6): 1: 2 for S1, S2, S3 and S4 samples, respectively. In other words, the ratios of glycine to metal nitrates (G/N) were 0.00, 0.67, 1.33 and 2.00 for S1, S2, S3 and S4 samples. The chemicals employed in the present work were of analytical grade supplied by Fluke Company.

2.2. Techniques

An X-ray measurement of various mixed solids was carried out using a BRUKER D8 advance diffractometer (Germany). The patterns were run with Cu K_α radiation at 40 kV and 40 mA with scanning speed in 2θ of 2 ° min^{-1}.

The crystallite size of $CoAl_2O_4$ present in the investigated solids was based on X-ray diffraction line broadening and calculated by using Scherrer equation [17].

$$d = \frac{B\lambda}{\beta \cos\theta} \qquad (1)$$

where d is the average crystallite size of the phase under investigation, B is the Scherrer constant (0.89), λ is the wave length of X-ray beam used, β is the full-with half maximum (FWHM) of diffraction and θ is the Bragg's angle.

Scanning electron micrographs (SEM) were recorded on SEM-JEOL JAX-840A electron microanalyzer (Japan). The samples were dispersed in ethanol and then treated ultrasonically in order disperse individual particles over a gold grids.

Energy dispersive X-ray (EDX) analysis was carried out on Hitachi S-800 electron microscope with an attached kevex Delta system. The parameters were as follows: accelerating voltage 10, 15 and 20 kV, accumulation time 100s, window width 8 μm. The surface molar composition was determined by the Asa method, Zaf-correction, Gaussian approximation.

3. RESULTS AND DISCUSSION

3.1. Structural analysis

The XRD diffractograms for S1, S2, S3 and S4 samples are given in Fig. 1.

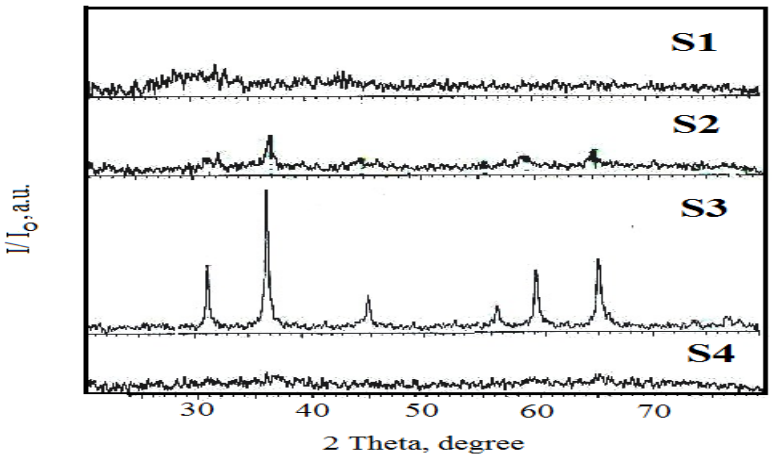

Figure 1. XRD patterns for the S1, S2, S3 and S4 samples.

Investigation of this figure revealed that: (i) The S1 and S4 sample consisted entirely of amorphous materials which may be cobalt and aluminum oxides and/or Co-Al- O compound. (ii) The S2 sample consisted of moderate crystalline $CoAl_2O_4$ particles as a single phase. This indicates that the presence of small amount of glycine (G/N = 0.67) led to stimulate the solid state between the reacting oxides yielding $CoAl_2O_4$ crystallites. (iii) In the XRD pattern for the S3 sample, the diffraction peaks of $CoAl_2O_4$ phase gradually become sharp and their intensities increase as the glycine content(G/N = 1.33) increases, revealing an increase of the size and amount of this phase. In other words, the increase in the glycine content enhances the solid state reaction between CoO and Al_2O_3 producing $CoAl_2O_4$ particles. (iv)The increase in the ratio of G/N from 1.33 to 2.00 resulted in formation of amorphous

materials. Finally, judicious adjustment of the metal precursor- to-fuel ratio can control the size and formation of $CoAl_2O_4$ nano-crystals.

3.2. The size control of $CoAl_2O_4$ nano- crystals

The change in the ratio of glycine to metal nitrates brought about an increase in the crystallite size (d) of $CoAl_2O_4$ nano- particles as shown in Table 1. In addition, Table 1 shows the lattice constant (a), unit cell volume (V) and X-ray density (D_x) of $CoAl_2O_4$ nano- particles depending upon the X-ray data.

Table 1. Some structural parameters of $CoAl_2O_4$ phase.

Samples	$CoAl_2O_4$			
	d (nm)	a (nm)	V (nm^3)	D_x (g/cm^3)
S2	22	0.8095	0.5305	4.4282
S3	26	0.8107	0.5327	4.4095

The increase in the amount of glycine during the preparation of the S3 sample brought about an increase in the values of crystallite size, lattice constant and unit cell volume of $CoAl_2O_4$ nano-crystals increase. On the other hand, this increase led to a decrease in the X-ray density (D_x) of $CoAl_2O_4$ nano-particles. The increase in the values of a, d and V could attributed to the incorporation of CoO ions in the lattice of Al_2O_3 crystallites yielding $CoAl_2O_4$ particles. This behavior resulted in an expansion in lattice constant depending upon the difference in the ionic radii between Co and Al species. On the other hand, the increase in the peak height of $CoAl_2O_4$ phase in the S3 sample could be attributed to the solid state reaction between CoO and Al_2O_3 yielding cobalt- aluminum compound. In addition, the decrease in the density due to the increase in glycine content could be ascribed to the reduction of oxygen vacancies which play a predominant role in accelerating densification i.e. the decrease in oxygen ion diffusion would retard the densification.

3.3. Formation of spinel $CoAl_2O_4$ compound

Solid state reaction between CoO and Al_2O_3 depending upon the thermal diffusion for the cations of these oxides resulted in formation of spinel-type $CoAl_2O_4$ compound [18]. Deraz reported that the glycine assisted combustion method is useful for providing an alternative of low cost mass production of various spinel materials [19, 20]. The counter-diffusion of Co^{2+} and Al^{3+} through a relatively rigid aluminates film led to the formation of $CoAl_2O_4$ particles. We speculate that the diffusing ions might be Co^{2+} including Co^{3+} on the basis of detecting Co^{2+} in the interface. In addition, following reactions indicate that Al_2O_3 decomposes to $2Al^{3+}$ and oxygen gas at Al_2O_3- interface.

Moreover, oxygen moves through the reacted area to be added to the CoO interface and form spinel by reacting with aluminum ions:

At Al_2O_3 interface:

$$3Al_2O_3 + 2Co^{2+} \rightarrow 2CoAl_2O_4 + 2Al^{3+} + 0.5O_2 \quad (2)$$

At CoO interface:

$$2Al^{3+} + 3CoO + 0.5O_2 \rightarrow CoAl_2O_4 + 2Co^{2+} \quad (3)$$

3.4. IR analysis

The IR transmission spectra for the samples S1, S2, S3 and S4 were recorded in the range of 1000- 350 cm^{-1} as shown in Fig. 2. It can see from this figure that the investigated method led to formation of spinel $CoAl_2O_4$ compound.

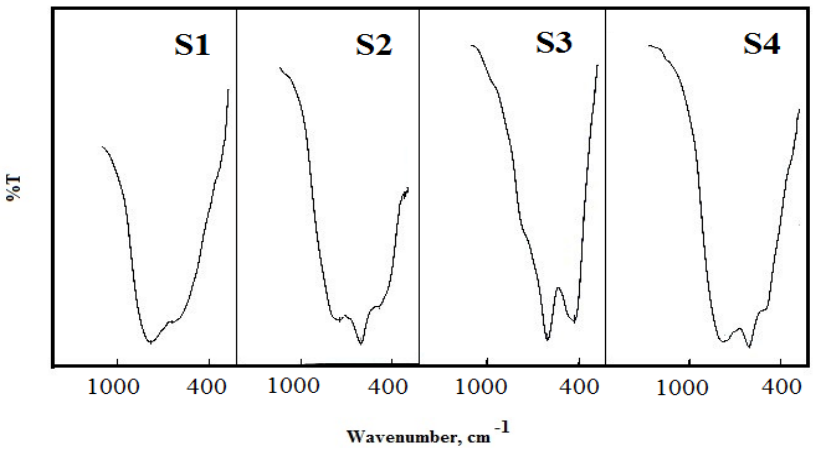

Figure 2. IR spectra for the S1, S2, S3 and S4 samples.

The IR bands for the as prepared solids are usually assigned to vibration of ions in the crystal lattice in the range of 1000- 350 cm^{-1}. Two main metal- oxygen bands are seen in the IR spectra of all spinels [21], namely tetrahedral (A-sites) and octahedral (B-sites) according to the geometrical configuration of nearest neighbors. The highest band υ_1, generally observed around 600 cm^{-1}, corresponds to intrinsic stretching vibrations of metal at the tetrahedral site, whereas the υ_2 lowest band, usually observed around 400 cm^{-1}, is assigned to octahedral- metal stretching. In inverse aluminates such as cobalt aluminates, the υ_1 and υ_2 bands are due to Al^{3+}-O^{2-} complexes present at A- and B-sites. The Co^{2+} ions occupy mainly the octahedral sites and fraction goes into tetrahedral sites [20]. This would explain the existence of a weak shoulder υ_1' around υ_1 band at 775±25 cm^{-1}. It can be seen from Fig. 2 that the difference in the intensities and positions of the absorption bands υ_1 and υ_2 is

referred to change in the nature of formation of cobalt aluminates by changing the glycine content. In fact, the intensities and positions of the absorption bands υ_1 and υ_2 depend strongly on the method and conditions of preparation. These results suggested that the change in the G/N ratio affect the formation of spinel cobalt aluminates.

3.5. Cation distribution

The intensities of the (2 2 0) and (4 4 0)) planes are more sensitive to the cations on tetrahedral, and octahedral, respectively [22]. Indeed, the Co^{2+} and Al^{3+} ions have a strong preference to occupy A and B sites, respectively [4]. Table 2 shows the observed intensities of the above planes.

Table 2. The intensity values of some hkl planes for the as prepared cobalt aluminates.

Samples	Peak height (a. u.)		
	I_{220}	I_{440}	I_{220}/ I_{440}
S2	06.6	10.5	0.629
S3	23.7	25.9	0.915

It can be observed that the intensity of the (2 2 0) and (4 4 0) planes increases as the G/N ratio increases. This infers that both Co^{2+} and Al^{3+} ions have preferentially occupied both the A and B sites. The maximum increase in the intensity of both (2 2 0) and (4 4 0) planes which attained 259.1% and 146.7%, respectively. This result might show that the solubility of CoO at A sites is greater than that at B sites involved in the cobalt aluminates lattice [4]. However, the substitution of some Al^{3+} ions by Co^{2+} ions at B site resulted in migration of these ions (Al^{3+}) from B site to A site. In other words, the increase in the glycine content led to an increase in the number of Co^{2+} ions on A site with subsequent increase in the crystallite size, lattice constant and unit cell volume of cobalt- aluminum compound. On the basis of the above data, the inverted spinel structure can be assigned in the synthesized materials having the formula $CoAl_2O_4$ can be expressed as:

$$(Al_x^{3+} Co_{1-x}^{2+})_A[Co_x^{2+} Al_{2-x}^{3+}]_B O_4^{2-} \qquad (4)$$

The parameter of inversion, x, is equal 0 for inverse spinel and to 1 when the spinel is normal.

The distance between the reacting ions (L_A and L_B), ionic radii (r_A, r_B) and bond lengths (A–O and B–O) on tetrahedral (A) sites and octahedral (B) sites of $CoAl_2O_4$ crystallites were calculated from the data of X-ray and also were tabulated in Table 3. It seen from this table that the increase in the G/N ratio brought about an increase in the calculated values of L_A, L_B, r_A, r_B, A–O and B–O of

$CoAl_2O_4$ crystallites. These observations confirm the increase in the crystallite size, lattice constant and unit cell volume of $CoAl_2O_4$ nano- particles.

Table 3. The values of L_A, L_B, A-O, B-O, r_A and r_B for the as prepared cobalt aluminates.

Samples	L_A (nm)	L_B (nm)	A-O (nm)	B-O (nm)	r_A (nm)	r_B (nm)
S2	0.3505	0.2862	0.1823	0.1983	0.0473	0.0633
S3	0.3510	0.2866	0.1825	0.1986	0.0475	0.0636

3.6. The morphology study

Figs. 3A-D shows the SEM images for S1, S2, S3 and S4 samples. The preparation method investigated brought about fabrication of spongy and fragile materials containing voids and pores. These voids and pores could be attributed to the release of large amounts of gases during combustion process due to decomposition of the glycine and Co and Al nitrates. In fact, the X-ray density of the S2 sample is lower than that of the S1 samples. It can be seen from the SEM images of the investigated solids that the agglomeration of the particles decreases as the G/N ratio increases. This indicates that the increase in the glycine content hinders the aggregation of the particles involved in the Co/Al nano-particles.

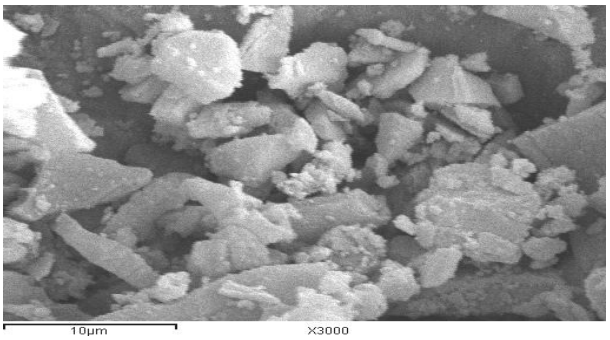

A

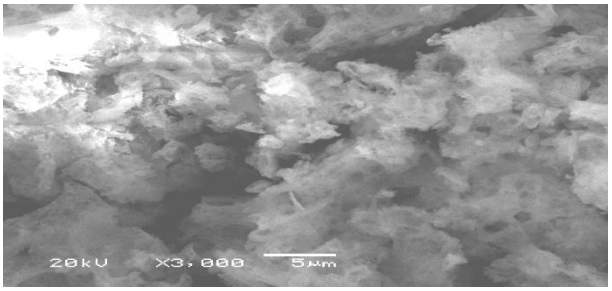

B

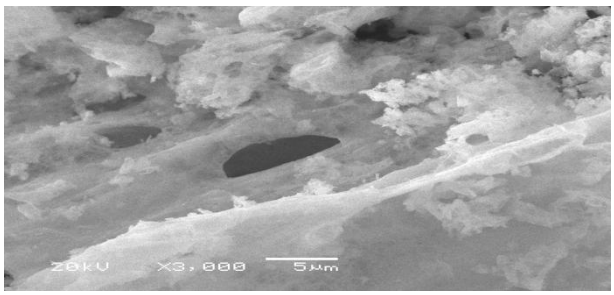

C

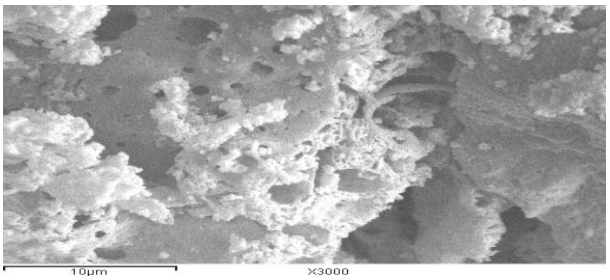

D

Figure 3. SEM images for the as synthesized samples; (A) S1, (B) S2, (C) S3 and (D) S4.

3.7. Homogeneity of the as prepared samples

Various areas on surface of the as prepared samples are considered by using energy dispersive X-ray (EDX) analysis at 20 keV. Tables 4 and 5 display the relative atomic abundance of O, Co and Al species present in the surface layers of The S2 and S3 samples, respectively. It can see from these tables that the surface concentrations of O, Co and Al species at 20 keV on different areas over the surface of specimens studied are much closed to each other. This indicates the homogeneous distribution of O, Co and Al species in the samples studied. So, the combustion route resulted in production of homogeneously distributed materials.

Table 4. The atomic abundance of elements measured at 20 keV and different areas over the S2 sample.

Elements	Area 1	Area 2	Area 3	Area 4
O	33.12	32.68	33.62	33.07
Co	42.66	44.03	41.15	42.82
Al	24.22	23.30	25.15	24.11

Table 5. The atomic abundance of elements measured at 20 keV and different areas over the S3 sample.

Elements	Area 1	Area 2	Area 3	Area 4
O	33.70	33.86	31.94	32.64
Co	40.89	40.40	46.27	44.13
Al	25.41	25.74	21.79	23.23

3.8. The elements gradient

Figures 4 and 5 showed the concentrations of Co, Al and oxygen species from the uppermost surface to the bulk layers for the S2 and S3 samples by using the EDX investigation at 5, 10, 15 and 20 keV.

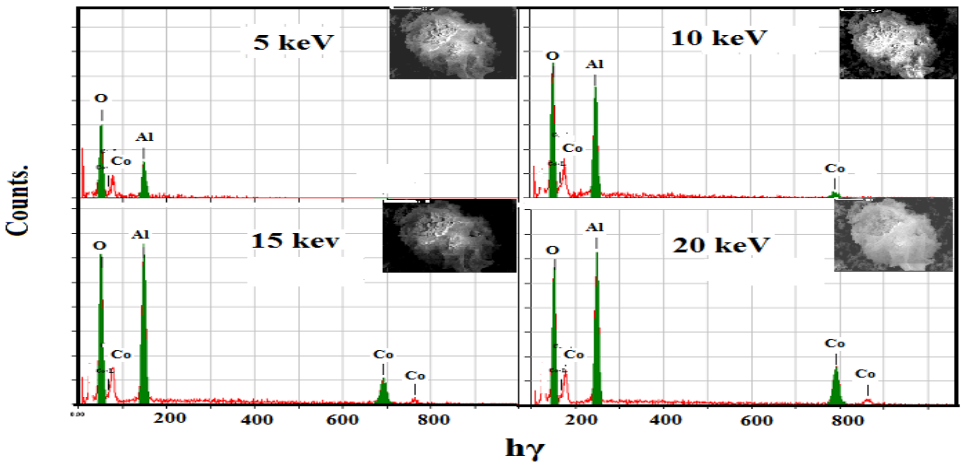

Figure 4. EDX pattern for the S1 sample at different applied voltages.

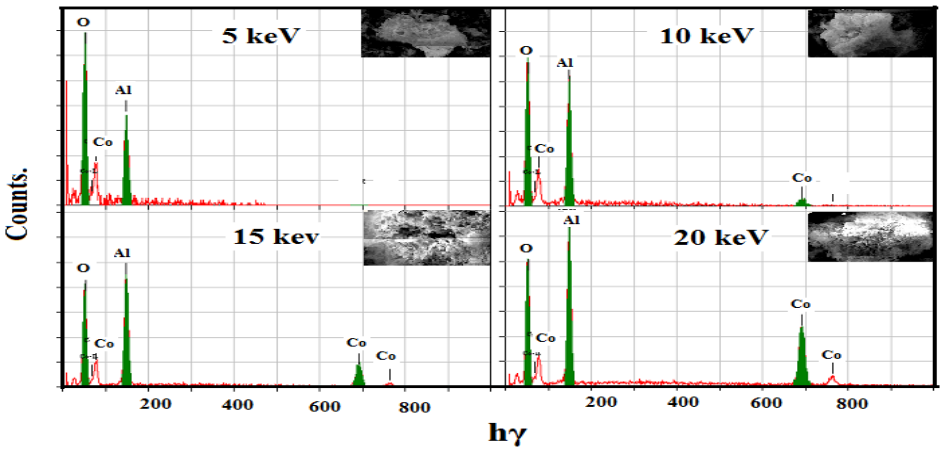

Figure 5. EDX pattern for the S1 sample at different applied voltages.

The values of concentrations of Co, Al and oxygen species at 5, 10, 15 and 20 keV for the S2 and S3 samples are summarized in Tables 6 and 7, respectively. Inspection of Tables 6 and 7 revealed that: (i) the surface concentrations of Al and oxygen species for the S2 and S4 samples decrease as the applied voltage increases from 5 to 20 keV. This indicates that the uppermost surface layer of the two prepared samples is O- and Al-rich layer. (ii) The absence of the Co species at uppermost surface layer of these samples. Indeed, the surface concentrations of Co species at 5 keV are zero for the S2 and S3 samples. The increase in the applied voltage above the previous limit (5 keV) showed that the surface concentrations of Co species increase from the uppermost surface layer to the bulk of the as prepared materials. These findings suggest a possible redistribution for the essential elements involved in the as synthesized cobalt aluminates with subsequent unique properties of these aluminates.

Table 6. The atomic abundance of elements measured at different voltages over the same area for the S2 sample.

Elements	Atomic abundance (%)			
	5 keV	10 keV	15 keV	20 keV
O	47.07	39.58	34.74	33.71
Co	00.00	06.08	37.72	40.85
Al	52.93	37.50	27.54	25.44

Table 7. The atomic abundance of elements measured at different voltages over the same area for the S3 sample.

Elements	Atomic abundance (%)			
	5 keV	10 keV	15 keV	20 keV
O	47.07	37.90	33.39	31.24
Co	00.00	28.05	41.84	48.41
Al	52.93	34.05	24.77	20.35

4. CONCLUSIONS

Effects of glycine content on the formation, structural and morphological properties of cobalt aluminates prepared by combustion method have been studied. The combustion route brought about the production of spinel $CoAl_2O_4$ nano- particles as a single phase. The increase in the glycine content

resulted in an increase in the crystallite size, lattice constant and unit cell volume of the produced cobalt aluminates. Opposite behavior was observed in the value of the X-ray density. The images of SEM showed that the as synthesized cobalt aluminates using high amounts of glycine has a significant porosity. The obtained samples have a homogenously distributed species in the whole mass prepared. The change in the G/N ration resulted in change in the surface concentrations of Co, Al and oxygen species involved in the cobalt aluminates.

ACKNOWLEDGEMENT
This project was supported by King Saud University, Deanship of Scientific Research, College of Science Research Centre.

References

1. D. G. Wickham, Inorganic Synthesis Vol. IX. Mc Graw Hill, New York, 152 (1967) 2449.
2. N. M. Deraz, Ph. D., Zagazig University, Zagazig, Egypt (1999).
3. N. M. Deraz, *Thermochim. Acta*., 401 (2003) 175.
4. O. M. Hemeda, M. A. Amer, S. Aboel- Enein, M. A. Ahmed, *Phys. Stat. Sol*., 156 (1996) 29.
5. R. Kalai Selvan, C. O. Augustin, L. John Berchmans, R. Saraswathi, *Mat. Res. Bull.*, 38 (2003) 41.
6. S. Bid and S.K. Pradan, *Materials Chemistry and Physics* 82 27 (2003).
7. R.E. Ayala and D.W. Marsh, *Ind. Chem. Res*. 30 55 (1991)
8. N. Ouahdi, S. Guillemet J.J. Demai, B. Durand L. Er. Rakho, R.Moussa and A.Samdi, *Material Letters* 95 334 (2005).
9. M. Zayat, D. Levy, *Chem. Mater*. 12 (2000) 2763.
10. Bolt, P. H., Habraken, F. H. P. M and Geus, J. W., *J. Solid. State Chem*. 135(1998)59.
11. S. Chokkaram, R. Srinivasan, D. R. Milburn, B. H. Davis, *J. Mol. Catal. A: Chem*. 121(1997)157.
12. U. L. Stangar,B. Orel, M. Krajnc, R. C. Korosec, P. Bukovec, *Materiali in Thechnologije*, 36(2002)387..
13. W. S. Cho, M. Kakihana, *J. Alloys Compd*. 287(999)87.
14. Z. Z. Chen, E. W. Shi, W. J. Li, Y. Q. Zheng, J. Y. Zhuang, B. Xiao, L. A. Tang, *Mater. Sci. Eng*. B107(2004)217.
15. N. M. Deraz, A. Alarifi, *Int. J. Electrochem. Sci.* 7(2012) 3798.
16. N. M. Deraz, A. Alarifi, *Int. J. Electrochem. Sci*7(2012) 3809.
17. B.D. Cullity, Elements of X-ray Diffraction, Addison-Wesly Publishing Co. Inc. 1976 (Chapter 14).
18. Cuiyan Wang, Shaomin Liu, Lihong Liu, Xuan Bai, *Materials Chemistry and Physics* 96 (2006) 361.
19. N. M. Deraz, *Ceramics International* 38 (2012) 511.
20. N. M. Deraz, *Int. J. Electrochem. Sci7*(2012) 4596.
21. R. D. Waldron, *Phys. Rev*.99 (1955) 1727.